Solution Structure of a Conformationally Restricted Fully Active Derivative of the Human Relaxin-like Factor[†,‡]

Erika E. Büllesbach,[*,§] Mathias A. S. Hass,[||,⊥] Malene R. Jensen,[||,@] D. Flemming Hansen,[||,#] Søren M. Kristensen,[||] Christian Schwabe,[§] and Jens J. Led[||]

Department of Biochemistry and Molecular Biology, Medical University of South Carolina, 173 Ashley Avenue, P.O. Box 250509, Charleston, South Carolina 29425, and Department of Chemistry, University of Copenhagen, Universitetsparken 5, DK-2100 Copenhagen Ø, Denmark

Received July 28, 2008; Revised Manuscript Received October 30, 2008

ABSTRACT: Analogous to insulin, the relaxin-like factor (RLF) must undergo a structural transition to the active form prior to receptor binding. Thus, the C-terminus of the B chain of RLF folds toward the surface of the central B chain helix, causing partial obliteration of the two essential RLF receptor-binding site residues, valine B19 and tryptophan B27. Via comparison of the solution structure of a fully active C-terminally cross-linked RLF analogue with the native synthetic human RLF (hRLF), it became clear that the cross-linked analogue largely retains the essential folding of the native protein. Both proteins exist in a major and minor conformation, as revealed by multiple resonances from tryptophan B27 and adjacent residues on the B chain helix. Notably, the minor conformation is significantly more highly populated in the chemically cross-linked RLF than it is in the hRLF. In addition, compared to the unmodified molecule, subtle differences are observed within the B chain helix whereby the cross-linked derivative shows a reduced level of hydrogen bonding and significant peak broadening at the binding site residue ValB19. On the basis of these observations, we suggest that the solution structure of the native hormone represents an inactive conformer and that a dynamic equilibrium exists between the C-terminally unfolded binding conformation and the inactive conformation of the RLF.

The relaxin-insulin family consists of eight structurally related hormones and growth factors: insulin (*1*), insulin-like growth factors (IGF) (*2*), relaxin (*3, 4*), relaxin-like factor (RLF,[1] also named insl3, or Ley-IL) (*5*), placentin (or insl4) (*6*), insl5 (*7*), insl6 (*8*), and insl7 (also named relaxin 3) (*9, 10*). With the exception of the insulin-like growth factors (IGFs), all proteins consist of two polypeptide chains, the A chain and B chain, held together by three disulfide bonds in conserved spacing. Two disulfide links connect the A and B chains, while the third disulfide bond appears within the A chain. Three-dimensional structures of insulin (*11*), IGF (*12, 13*), relaxin (*14, 15*), and the relaxin-like factor (RLF) (*16*) indicate that the intra-A chain disulfide bond stabilizes the A chain loop and the two antiparallel short helical segments located in the N- and C-terminal region of the A chain. In all structures, a longer helix is found in the midregion of the B chain, which often is followed by a β-turn. Functionally the hormones are quite diverse; for instance, insulin and IGF exhibit their metabolic/growth promoter function by acting through tyrosine-kinase receptors (*17*−*19*), whereas relaxin and the RLF stimulate tissue remodeling through seven-transmembrane G-protein-coupled receptors (*10, 20*−*22*).

The RLF is a critical regulator of sexual differentiation that mediates intra-abdominal migration of the testes in the developing male (*23*). The protein isolated from bovine testis consists of a 26-amino acid residue A chain and a 41-residue B chain and is significantly larger than insulin or relaxin. In its native form, the binding affinity for the receptor appears to be reduced when compared to that of a shorter form deduced from the cDNA sequence (*24*) in which the B chain consists of the 31 N-terminal residues. While this form is almost exclusively used in structure and function studies, it has been shown that the C-terminus of the RLF B chain can be shortened even further to 27 residues, ending in TrpB27 amide (*25*).

[†] This work was supported by Grants GM 48893 and 1-R01-HD40406 from the National Institutes of Health, the Medical University of South Carolina, Research Committee, Danish Agency for Science, Technology and Innovation Grants 9400351, 9801801, 26-03-0055, 21-04-0519, and 272-07-0466, Carlsbergfondet Grant 1624/40, Novo Nordisk Fonden Grant 2003-11-28, and Villum Kann Rasmussen Fonden Grant 8.12.2003.

[‡] Structures are deposited in the Protein Data Bank as entries 2k6t for the human RLF and 2k6u for the cross-linked RLF derivative.

* To whom correspondence should be addressed: Department of Biochemistry and Molecular Biology, Medical University of South Carolina, 173 Ashley Ave., P.O. Box 250509, Charleston, SC 29425. Telephone: (843) 792-9926. Fax: (843) 792-4850. E-mail: bullesee@musc.edu.

[§] Medical University of South Carolina.

[||] University of Copenhagen.

[⊥] Present address: Leiden Institute of Chemistry, Leiden University, Gorlaeus Laboratories, P.O. Box 9502, 2300 RA Leiden, The Netherlands.

[@] Present address: Institut de Biologie Structurale Jean-Pierre Ebel, 41 Rue Jules Horowitz, 38027 Grenoble, France.

[#] Present address: Department of Medical Genetics and Microbiology, University of Toronto, 1 King's College Circle, Toronto, ON, M5S 1A8 Canada.

[1] Abbreviations: ARIA, Ambiguous Restraints for Iterative Assignment; DQF-COSY, double-quantum-filtered correlation spectroscopy; GPCR, G-protein-coupled receptor; HSQC, heteronuclear single-quantum coherence; INSL3, insulin-like 3; LGR8, leucine-rich G-protein-coupled receptor-8; NMR, nuclear magnetic resonance; NOE, nuclear Overhauser effect; NOESY, nuclear Overhauser effect spectroscopy; RLF, relaxin-like factor; hRLF, human relaxin-like factor; TOCSY, total correlation spectroscopy; WATERGATE, water suppression through gradient-tailored excitation.

10.1021/bi801412w CCC: $40.75
Published on Web 11/20/2008

The RLF binds leucine-rich G-protein-coupled receptor 8 (LGR8) with remarkable affinity ($K_d = 0.1$ nM) (*26*) despite the lack of a sharply defined binding site (*16, 27, 28*). Single-residue replacements (*16, 25, 28, 29*) revealed that the side chains of ArgB16, ValB19, and TrpB27 are important but made it clear that the sum of individual side chain contributions of RLF does not account for the observed high-affinity binding constant. In contrast, multiple replacements of these same residues or of residues adjacent to the binding residues caused an effect that was significantly larger than the sum of the effects of single replacements. This implies that the proper orientation of other, secondary binding sites is necessary for receptor binding (*16, 28*). Such a mechanism of RLF−receptor interaction should allow one to "freeze" the molecule in a purported active conformation. In a previous paper, we reported on the synthesis and properties of a series of derivatives containing cross-links of variable lengths between the side chain in position B26 and the C-terminus of the A chain. The results of that study led to the conclusion that the distance between the two chains is critical for hormonal activity. Accordingly, cross-linked RLFs bearing either a glycine or a β-alanine spacer are fully active, while direct linking of the A chain C-terminus and lysine B26 led to a loss of 97% of receptor binding capacity (*25*). In addition, it was found that the average position of side chains varied considerably in the differently cross-linked RLFs and that the restriction of motion of TrpB27 by cross-linkers of various lengths influences the activity of the hormone. These observations pointed to the exciting possibility that the different cross-links freeze the RLF at various distances from its binding conformation. We have determined the solution structure of a C-terminally cross-linked RLF analogue that is fully active. As suggested by our analysis of the structure of the analogue as well as the native RLF, both proteins must undergo a structural transition to the active form prior to receptor binding.

MATERIALS AND METHODS

Materials. The human RLF (hRLF) and ^{15}N(GlyB23, GlyB24, AlaA2, AlaA7, GlyA14)-labeled hRLF were synthesized as previously described (*29*). The cross-linked human RLF consisted of a 26-residue A chain extended C-terminally by glycine A27 and a 27-residue B chain with arginine B26 replaced with lysine with an amidated C-terminus. The ε-amino group of lysine B26 and the carboxyl group of glycine A27 were condensed to establish an isopeptide cross-link between the A and B chains. The synthesis has been published (*25*).

NMR Spectroscopy. The protein was dissolved in 40 mM perdeuterated acetic acid/NaOD (pH 5.0) in water containing 8% D_2O or in D_2O. NMR tubes were sealed under nitrogen shortly after sample preparation. NMR experiments were conducted at a magnetic field strength of 18.7 T using a Varian Unity Inova 800 spectrometer equipped with a cryoprobe. The water signal was suppressed either by selective excitation of the water resonance (WATERGATE) (*30*) or by presaturation of the residual HDO resonance of samples in D_2O. In all experiments, the carrier frequency was set at the center of the spectrum at the water resonance. Three different types of two-dimensional ^{1}H−^{1}H correlated NMR experiments were conducted: DQF-COSY (*31*), NOESY (*32, 33*), and TOCSY (*34, 35*). ^{1}H−^{13}C HSQC spectra of the aliphatic region were acquired at a magnetic field strength of 18.7 T. The sweep width was 12 kHz in the ^{1}H dimension and 16 kHz in the ^{13}C dimension. Spectra were processed using NMRPipe (*36*), while spectral analyses were carried out with SPARKY (by T. D. Goddard and D. G. Kneller, SPARKY 3, University of California, San Francisco).

For hRLF TOCSY and NOESY, conditions were optimized by recording spectra with different mixing times (40, 60, 80, and 100 ms for TOCSY; 80, 120, and 200 ms for NOESY) and temperatures (20, 23, 28, 30, 33, 35, and 40 °C). The optimized conditions (mixing times of 60 ms for TOCSY and 120 ms for NOESY) and temperatures of 25, 30, and 35 °C were applied for the cross-linked RLF. Severe ambiguities in peak assignments were resolved by evaluating spectra at different temperatures. To investigate intermolecular interactions, a series of NOESY spectra of hRLF were recorded at 35 °C and pH 5.0 at concentrations of 1.2, 0.6, 0.3, 0.2, and 0.1 mM. The number of scans per FID was increased throughout the concentration series from 16 scans at the highest concentrations to 64 scans at the lowest.

Structure Calculations. Sequential assignment was accomplished using the strategy described by Wüthrich (*37*). Most spin systems were identified, but AlaA7 was assigned only after ^{15}N-labeled amino acids were incorporated into hRLF positions GlyB23, GlyB24, AlaA2, AlaA7, and GlyA14. ^{1}H−^{15}N HSQC and ^{1}H−^{15}N HSQC-NOESY experiments were conducted to identify proton resonances of the amide and methyl groups. For structure calculations, interproton distance restraints were obtained from NOESY spectra at 35 °C and a mixing time of 120 ms. Deuterium exchange experiments at pH 5.0 and 35 °C failed due to fast exchange of all amide protons, indicating the presence of a significant population of partially unfolded structures besides the folded form. However, at pH 2.7 and 15 °C, slowly exchanging protons were identified and were essentially identical to backbone amides of helical segments as predicted by the chemical shift index (*38*) and by the amide proton temperature coefficients (*39*). Thus, α-helices B12−B21, A5−A12, and A17−A22 were predicted, and 13 H-bond restraints were included in the calculations.

H^N−H^A coupling constants for the hRLF were determined by a combination of linear predictions and least-squares analyses (*40*). The φ angles in predicted helical regions could not be resolved by this procedure but were predicted using PREDITOR (*41*). For the hRLF, 20 coupling constants and 22 predicted φ and 19 predicted ψ torsion angles were included in the final calculations, whereas for the cross-linked RLF, 25 predicted φ and 18 predicted ψ bond angles were used. On the basis of intraresidue NOE intensities (*42*), 12 and 8 χ torsion angles were included for the hRLF and cross-linked RLF, respectively.

ARIA (Ambiguous Restraints for Interactive Assignment, version 2.0 or 2.1) (*43*) in combination with CNS (*44*) was used for structure calculations. The input consisted of two NOESY spectra acquired in H_2O and D_2O at pH 5.0 and 35 °C with a mixing time of 120 ms. The data set recorded in H_2O included all resonances involving aromatic side chains and amide protons, whereas the data set recorded in D_2O included only resonances between aliphatic protons. Peaks were selected on one side of the diagonal only to ensure

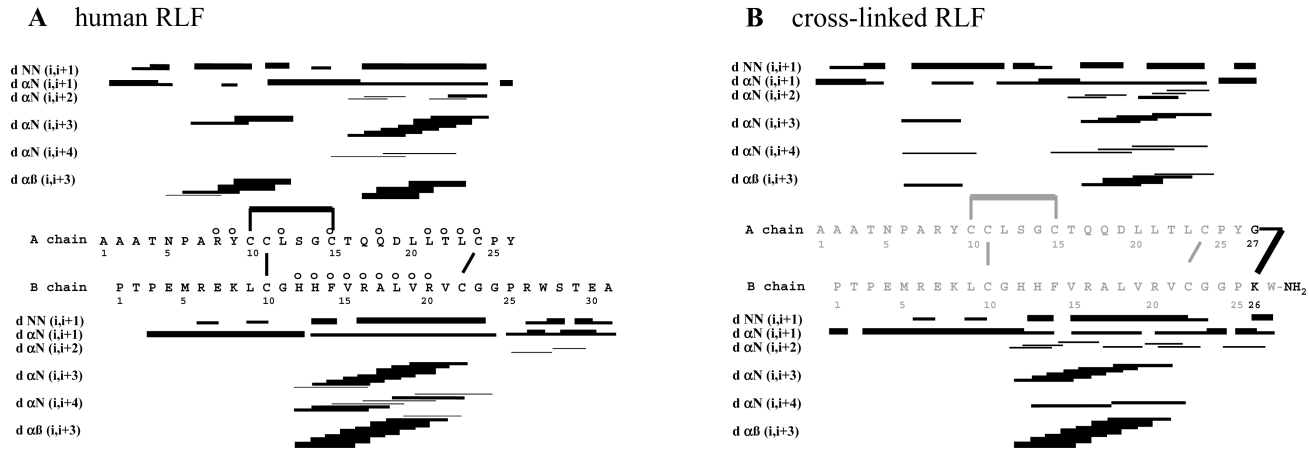

FIGURE 1: Sequential and medium-range NOE connectivities in the human RLF (A) and cross-linked RLF (B). The cross-linker consists of lysine replacing arginine at position B26 and an iso-peptide bond between the lysine side chain amino group and the carboxyl group of the glycine extension of the A chain. Glycine in position A27 serves as a spacer. The intensity of the NOE connectivities is indicated by the thickness of the bars: distances of <3 Å (thick), 3−4 Å (medium), and >4 Å (thin). Circles indicate slowly exchanging amide protons.

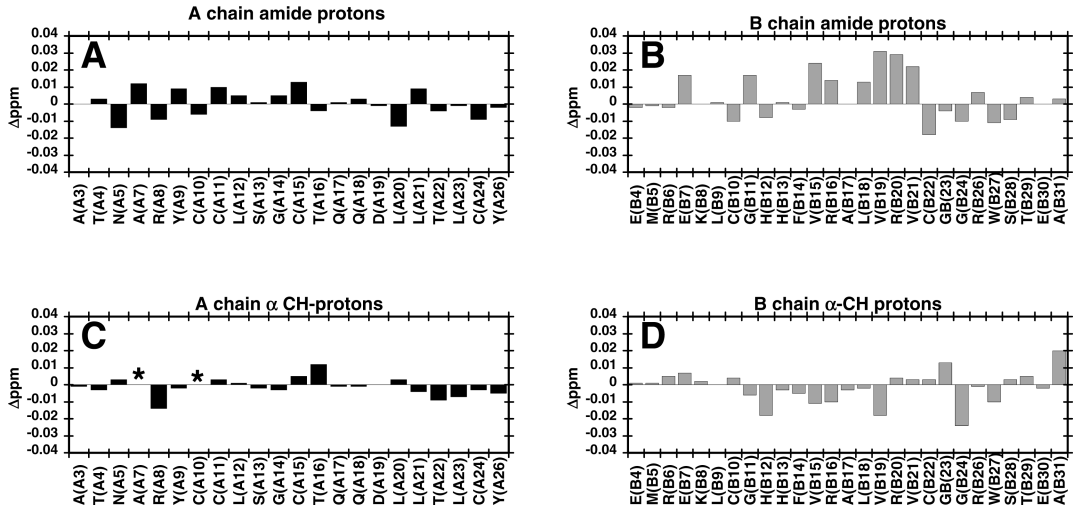

FIGURE 2: Chemical shift changes upon dilution of the hRLF (pH 5.0 and 35 °C). $\Delta ppm = CS_{1.2\ mM} - CS_{0.2\ mM}$. (A) Amide protons of the A chain, (B) amide protons of the B chain, (C) α-protons of the A chain, and (D) α-protons of the B chain. Glycine HA2 and HA3 were averaged. Asterisks indicate no data.

unique entry. In addition, all spectra were carefully screened and artifacts were excluded. This measure reduced the number of both merging and rejected NOEs during the structure calculation and eased the evaluation of those peaks. Unambiguous long-range and medium-range NOEs were preassigned.

For iterations 0−8 in the ARIA calculations, the violation tolerance was set at 1000, 5, 3, 1, 1, 1, 0.5, 0.3, and 0.3 Å, respectively. The frequency windows were set to 0.026 and 0.013 ppm in the F_1 and F_2 dimensions, respectively. This setting eliminated the frequency of merging unrelated peaks and reduced the NOEs rejected by the program (*45*) (30 for the hRLF and six for the cross-linked RLF).

RESULTS

The structures of the hRLF and the fully active C-terminally cross-linked RLF derivative were obtained from the experimental NMR data and compared. The cross-link was constructed by extending the C-terminus of the A chain by glycine A27 and by replacing arginine B26 in the B chain with lysine. Condensation of the carboxyl group of GlyA27 to the side chain amino group of LysB26 established a permanent cross-link within the C-terminal region of the molecule. The sequences of the hRLF and the cross-linked analogue are displayed in Figure 1.

Sample conditions and spectral parameters were optimized for the human RLF and subsequently applied to the cross-linked derivative. CD spectroscopy in the far-UV region indicated that secondary structure changes occur below pH 3.0 (Figure S2 of the Supporting Information). On the other hand, at neutral pH, the solubility in water was reduced to approximately 0.1 mM. We have chosen pH 5.0 because at this pH the hRLF retains a high solubility (>1.2 mM) and because amide proton exchange is slower than it is at physiological pH while the native conformation is maintained as judged by the far-UV CD measurements.

Backbone chemical shifts within a concentration series for the hRLF showed that concentration-dependent differences were small, with the largest shifts observed (0.02−0.04 ppm) for amide protons of ValB15, ValB19, ArgB20, and ValB21 and the α-protons of GlyB24 (Figure 2). The small changes in chemical shift indicate a weak self-association of the RLF. This was confirmed by hydrodynamic measurements based on ^{15}N NMR relaxation (Figure S3 of the Supporting

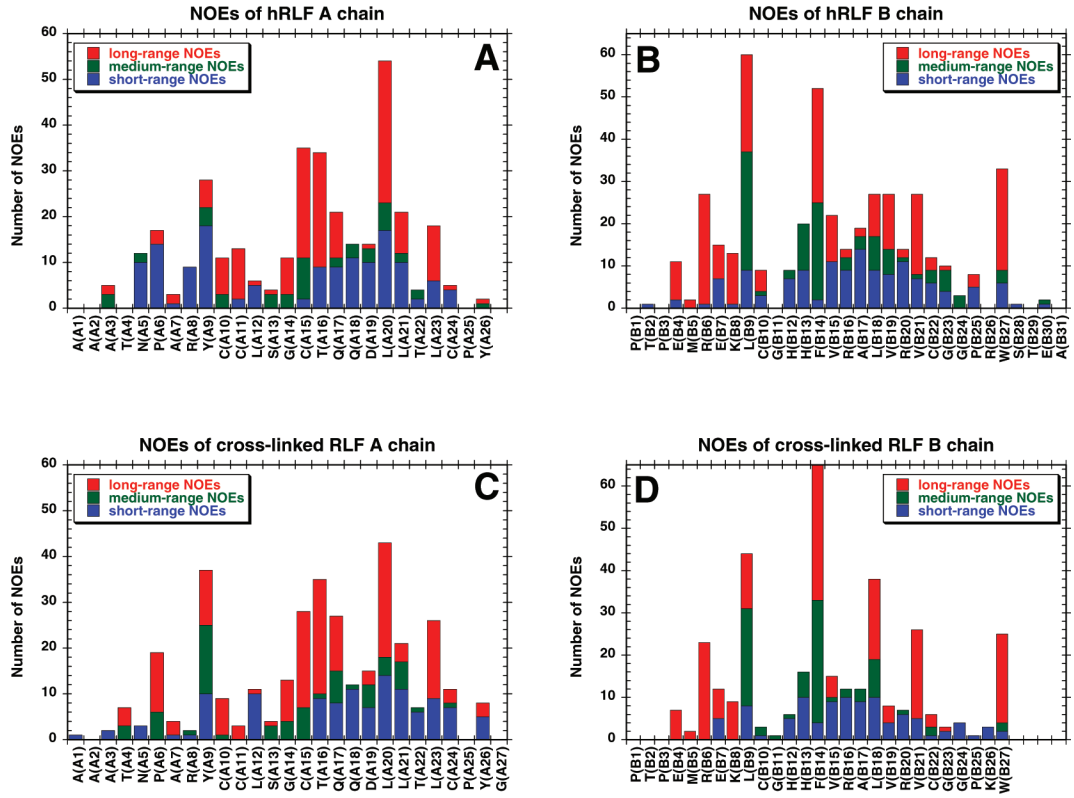

FIGURE 3: Display of short-range NOEs (sequence separation of two to three residues), medium-range NOEs (sequence separation of four to five residues), and long-range NOEs (sequence separation of more than five residues). NOEs between GlyA27 and LysB26 were considered sequential: (A) hRLF A chain, (B) hRLF B chain, (C) cross-linked RLF A chain, and (D) cross-linked RLF B chain.

Information). Close inspection of the NOESY spectra did not reveal any specific concentration-dependent cross-peaks that would be indicative of intermolecular interactions. The structure of both proteins was predicted on the basis of the NOESY spectra that were recorded at a protein concentration of 1.2 mM. The structures were calculated using ARIA, an interactive protocol for simultaneous NOE assignment and structure calculation (*43*).

Structure of the Human RLF. The chemical shifts of the amide protons were well dispersed, ranging from 9.7 ppm for ThrA16 to 7.0 ppm for PheB14/ValB15. Sequential, short-range, and medium-range NOEs (Figure 1A) provide clear evidence for the presence of α-helices in the C-terminal region of the A chain (residues GlnA17−ThrA22) and the midregion of the B chain (residues HisB12−ValB21). With the α-protons and α-carbons of AlaA7 and CysA10 unassigned, the presence of the helix in the N-terminal region of the A chain (ProA6−LeuA12) was established by the slow hydrogen exchange rates for the NH protons of residues ArgA8, TyrA9, and LeuA12, by chemical shift-based calculations of the temperature coefficients for backbone amide protons (*39*), and by torsion angle predictions (*41*). Long-range NOEs between residues LeuB9, PheB14, AlaB17, and ValB21 of the B chain and ProA6, AlaA7, CysA10, CysA15, LeuA20, and LeuA23 of the A chain are indicative of a hydrophobic core (Figure 3A,B). The relative orientation of the two antiparallel A chain helices is deduced from NOEs between the side chains of ProA6 and LeuA23 and by additional long-range NOEs between the phenol ring of TyrA9 and side chains of residues located in the N-terminal region of the A chain (residues AlaA3 and ThrA4), in the midregion of the A chain (residues CysA15 and ThrA16), and in the C-terminal region of the A chain (residue LeuA23). Numerous NOEs were observed between the N-terminal segment of the B chain (Arg-Glu-Lys, B6−B8) and the midregion of the A chain (Gly-Cys-Thr, A14−A16). As reported by Rosengren et al. (*16*), two different signals were observed for the N-terminus of the B chain (B1−B6), probably representing trans and cis isomers of the ThrB2−ProB3 bond. The C-terminus of the B chain folds back to the midregion of the B chain, as signified by NOEs between the indole ring protons of TrpB27 and the methyl groups on the surface of the B chain helix (ValB15, LeuB18, and ValB19). The overall structure is similar to that reported by Rosengren et al. (*16*). However, the indole side chain of TrpB27 in our structure is differently oriented and more restricted in its position. Thus, long-range NOEs were observed between all aromatic protons of the indole ring and the methyl groups of ValB19, between all protons of the phenyl ring and the methyl groups of ValB15, and between protons H2 and Z2 of the indole ring and the methyl groups of LeuB18. Together, these NOEs indicate that the active site residue TrpB27 is closer to the other active site residue, ValB19, and to residues ValB15 and LeuB18, than reported previously (*16*).

Structure of the Cross-Linked RLF. The overall spectral features of the C-terminally cross-linked RLF are similar to those of the native RLF. This includes the dispersion of the backbone amide resonances and the observation of multiple resonances for residues B1−B6. However, resonances display an increased level of line broadening, reducing the total number of evaluated NOEs compared to that of the hRLF (Table 1). In the N-terminal region of the A chain (Figure 1B), only few medium-range NOEs indicative of an α-helix could be identified. Medium- and long-range NOEs (Figure 3C) persisting between the side chain of TyrA9 and AlaA3,

Table 1: NMR Statistics for Structural Ensembles of the hRLF and Cross-Linked RLF[a]

	hRLF	cross-linked RLF
NOEs	1025	942
unambiguous	913	828
intraresidue	412	392
inter-residue		
sequential (1)	202	176
short-range (2−3)	109	76
medium-range (4−5)	53	41
long-range (>5)	137	143
ambiguous	82	108
two resonances	73	101
three resonances	7	6
four resonances	2	1
total	995	936
no. of H-bonds	13	13
^3J coupling	21	
no. of dihedral angle restraints		
ϕ	22	25
ψ	19	18
χ	12	8
no. of violations		
NOEs and H-bonds (>0.5 Å)	0.2	0.6
dihedral angles (>5°)	1.60	4.15
J coupling (>1 Hz)	0.65	−
rmsd (mean ± standard deviation)		
NOEs (Å)	0.053 ± 0.0015	0.048 ± 0.0075
bond lengths (Å)	0.0056 ± 0.0002	0.0042 ± 0.0019
bond angles (deg)	0.73 ± 0.02	0.62 ± 0.028
impropers (deg)	0.54 ± 0.025	0.40 ± 0.028
average pairwise root-mean-square deviation		
helix A6−11 backbone (Å)	0.39 ± 0.26	0.42 ± 0.039
helix A12−23 backbone (Å)	0.14 ± 0.04	0.44 ± 0.11
helix B13−21 backbone (Å)	0.14 ± 0.04	0.28 ± 0.04
all backbone atoms (Å)	1.92 ± 0.37	0.95 ± 1.25
Ramachandran analysis[b]		
most favored (%)	69.8 ± 5.8	75.5 ± 5.1
allowed (%)	24.2 ± 5.7	21.7 ± 4.7
generously allowed (%)	3.2 ± 1.8	0.96 ± 1.2
disallowed (%)	2.8 ± 1.9	2.0 ± 1.6

[a] The evaluation is based on the 20 lowest-energy structures. [b] After refinement in water.

GlyA14, CysA15, ThrA16, AspA19, and LeuA23 are indicative of a folded structure. In addition, predictions based on chemical shift data (*38, 39, 41*) suggest the presence of an α-helical segment for the sequence from ProA6 to LeuA12, as well as for the segments of GlnA17−ThrA22 and HisB12−ValB21 in the cross-linked derivative. Long-range intra-A chain NOEs are more frequent in the cross-linked RLF than in the hRLF, in particular, NOEs between ProA6 and LeuA23 as well as between TyrA9 and LeuA23. These additional NOEs are of no apparent consequence for the overall fold of the A chain. Fewer long-range NOEs were recorded for the mid- to C-terminal region of the B chain of cross-linked RLF as compared to the hRLF (Figure 3). The cross-link (LysB26−GlyA27) itself gave rise to intraresidue, sequential, and short-range NOEs, indicating that the link does not interfere with the overall fold of the protein and that it does not contribute to the structure other than restricting the distance between the C-terminal ends of the two chains.

Comparison of the Human RLF and Its Cross-Linked Derivative. Comparison of the chemical shift values of the spectra of the two proteins shows only small differences (Figure 4). As expected, the largest deviations are observed around the position of the restricting cross-link within the C-terminal region of both chains (GlyB23−TrpB27 and LeuA23−TyrA26). Interestingly, the effect propagates mostly along the surface of the B chain helix affecting (Δ > 0.05 ppm) the amide protons of CysB10, GlyB11, HisB12, ValB15, LeuB18, ValB19, and ArgB20 and the α-hydrogen of HisB12. The largest difference exceeding 0.1 ppm was recorded for the amide protons of ValB15 and LeuB18. In contrast, hydrophobic core residues PheB14, AlaB17, and ValB21 are less affected or not affected by the modification. Within the A chain, the differences were most pronounced (Δ > 0.05 ppm) for the cysteine amide protons of A10, A11, and A15 and for the α-proton of LeuA23. These small chemical shift differences do not reflect any difference in the secondary structure as predicted by the chemical shift index (Figure 5).

Temperature coefficients less negative than −4.25 ppb/K are indicative of hydrogen-bonded amide protons (*39*). Accordingly, hydrogen bonds were predicted for amide protons of PheB14−ValB21, suggesting the presence of the B chain helix (HisB12−ValB21) as shown in Figure 6. Both helices of the A chain are predictable in a similar way, although with less certainty. The positive values for the temperature coefficients for PheB14, CysA11, and GlyA14 suggest that these amide protons are located in a hydrophobic environment (*39*). It is noteworthy that all but the temperature coefficient for TyrA26 are more negative for the cross-linked RLF than for the hRLF, indicating weaker hydrogen bonds and hence reduced stability and increased flexibility of the structure of the derivative. In fact, for the cross-linked RLF, temperature coefficients for ValB15, AspA19, LeuA20, and LeuA21 are below the threshold, whereas the temperature coefficients for ArgB20 and ValB21 are at the threshold for α-helix-stabilizing hydrogen bonds (Figure 6).

From the NOEs, we can conclude that the aromatic side chains of TrpB27 in the C-terminal region of the native and cross-linked protein have different orientations with respect to the B chain helix. Thus, in the cross-linked derivative, only NOEs between indole protons HD1 and HE3 and the ValB19 methyl groups are retained, whereas new NOEs appear between phenyl ring protons E3 and Z3 and the methyl groups of LeuB18. In addition, one methyl group of LeuB18 is upfield shifted by 0.12 ppm. Consequently, the TrpB27 indole ring in cross-linked RLF occupies a position different from that in the native RLF, which affects mostly the location of the phenyl moiety while the pyrrole rings of the two proteins are in similar positions relative to the rest of the protein (Figure 7). This result is in agreement with the previously reported quenching of the tryptophan fluorescence in this cross-linked analogue (*25*). With the altered position of the indole ring in the cross-linked RLF, the methyl groups of ValB19 are now more solvent-exposed.

Both the hRLF and the cross-linked RLF exhibit multiple resonances for a series of residues on the B chain, suggesting at least two conformations. The residues showing multiple resonances are TrpB27 and residues ValB15, ValB19, and ValB21 on the B chain helix. For TrpB27, the relative intensities of the resonances corresponding to the two conformations are similar for both proteins (Figure 8). In addition, the relative intensities of the corresponding resonance in the two conformers are different for the three valine residues on the B chain helix that show double signals. Thus, for each of the valines, at least two different spin systems coexist in which chemical shifts are markedly different for the α- and γ-protons. For instance, the intensities of the main

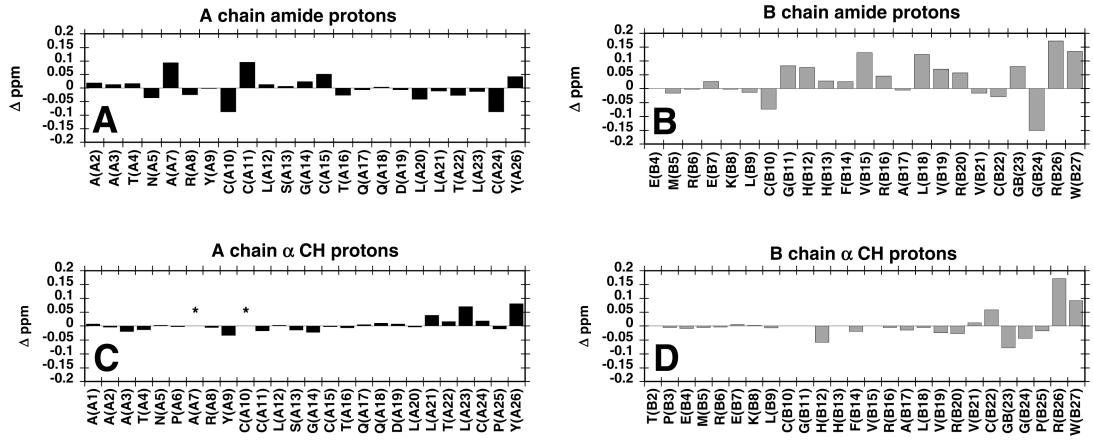

FIGURE 4: Chemical shift differences between the hRLF and cross-linked hRLF each at 1.2 mM, pH 5.0, and 35 °C [Δppm = CS_{hRLF}(ppm) − $CS_{cross\text{-}linked}$(ppm)]. (A) Backbone amide protons of the A chain, (B) backbone amide protons of the B chain, (C) α-protons of the A chain, and (D) α-protons of the B chain. Glycine HA2 and HA3 were averaged. Asterisks indicate no data.

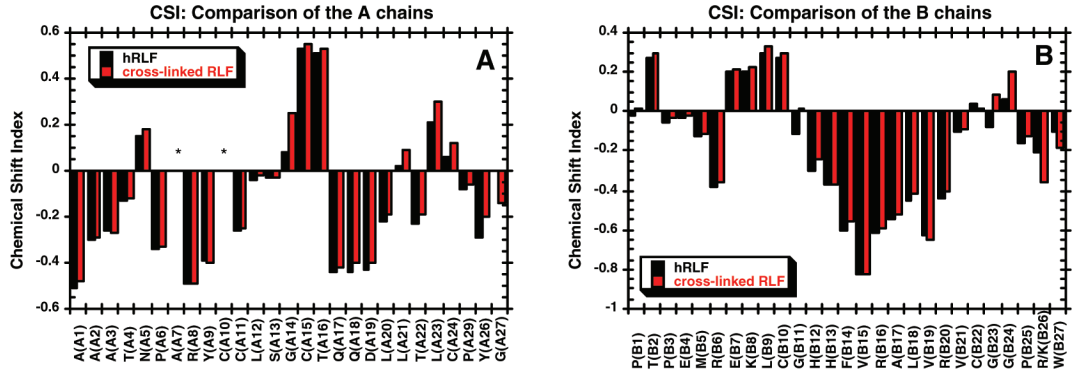

FIGURE 5: Proton chemical shift indices of the hRLF (black bars) and cross-linked hRLF (red bars): (A) A chain residues and (B) B chain residues. Asterisks indicate no or incomplete data.

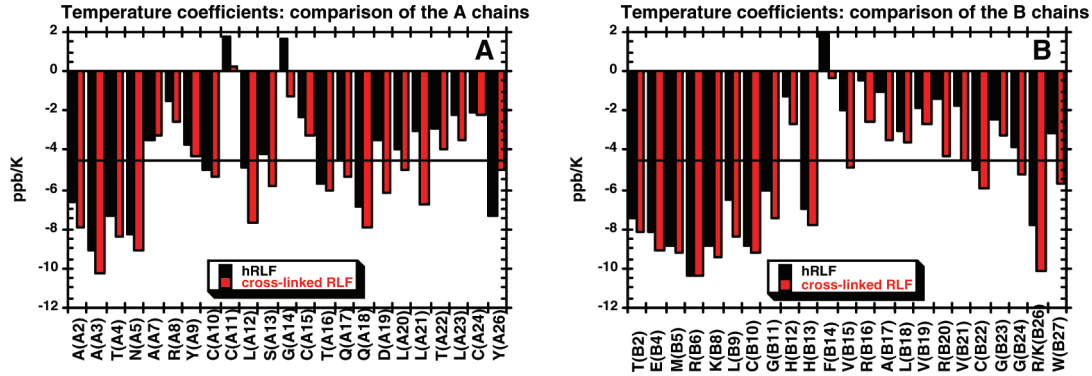

FIGURE 6: Temperature coefficients for the backbone amides of hRLF (black) and cross-linked RLF (red). Temperature coefficients less negative than −4.25 ppb/K (line) imply the existence of hydrogen bonds: (A) A chain residues and (B) B chain residues.

HA−HG resonances for ValB15 in the hRLF and cross-linked RLF are 90% and 73%, respectively; for ValB21, the main resonance constitutes 98% in the hRLF and is slightly asymmetrical, while it constitutes only 76% in the cross-linked derivative and is symmetrical. In the case of ValB19, the HA−HG resonances in the TOCSY spectrum show two distinct double signals in a 1:5 ratio for the hRLF, but in the cross-linked derivative, the main two resonances have collapsed to a diffuse peak (Figure 9). No sequential NOEs could be established between the signals corresponding to the minor forms, and the different conformers were identified by only their different signals in the TOCSY spectra (Figures 8 and 9) and by the multiplicity of the $^{1}H-^{13}C\alpha$ resonances in the $^{1}H-^{13}C$ HSQC spectra. The subsequent structures were calculated using the main resonances (Figure 10). However, the fact that multiple signals are observed shows that both the RLF and the cross-linked RLF assume two different conformations around TrpB27, corresponding to a major and a minor conformation. Moreover, we find that the population of the minor conformation is higher in the cross-linked RLF than in the hRLF. On the basis of these observations and the fact that the cross-linked RLF investigated here is the analogue with the highest activity among those examined previously (*25*), we suggest that the minor conformation corresponds to the conformation that the RLF must assume to bind to its receptor, as discussed in detail below.

DISCUSSION

Alanine scanning of the RLF has led to the identification of the side chains of ArgB16, ValB19, and TrpB27 as

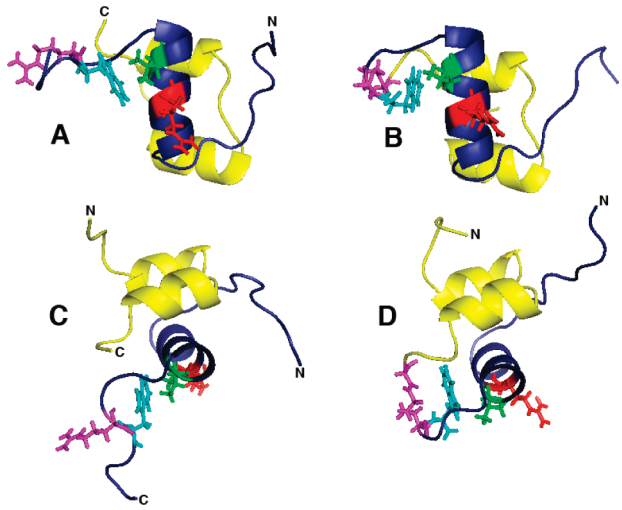

FIGURE 7: Comparison of the hRLF and cross-linked RLF. Views of the hRLF (A) and cross-linked RLF (B) from the surface of the B chain helix. Views of the hRLF (C) and cross-linked RLF (D) through the B chain helix. Blue is used for the B chain helix, yellow for A chain helices, red for ArgB16, green for ValB19, magenta for position B26 in the hRLF and positions B26 and A27 in the cross-linked RLF, and cyan for TrpB27. N marks an N-terminus, and C marks a C-terminus.

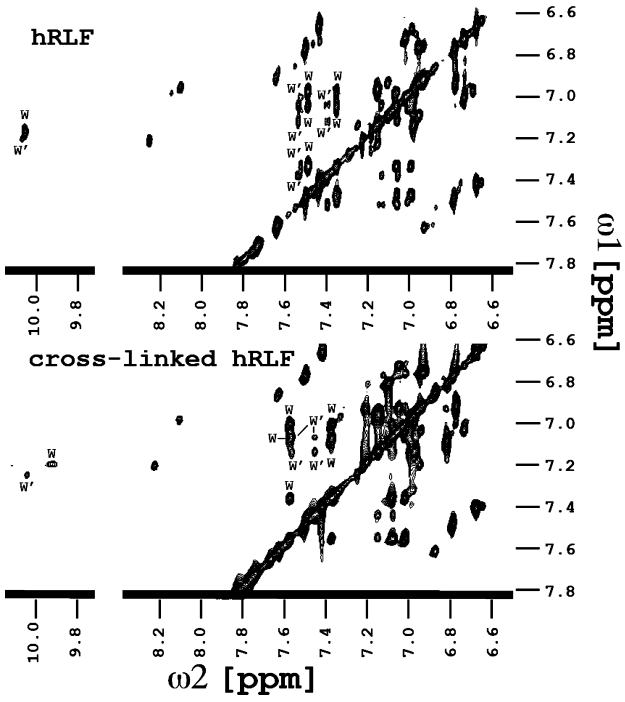

FIGURE 8: Regions of the TOCSY spectra of the hRLF (top) and cross-linked RLF (bottom) showing the chemical shifts and the multiplicity of the aromatic cross-peaks for TrpB27. W is the TrpB27 major form and W′ the TrpB27 minor form.

receptor binding residues (*16, 28*). B chain truncation, tryptophan substitution, and steric displacement experiments have shown that tryptophan B27 is essential for binding (*29*). Thus, deleting the C-terminal region of the B chain, including TrpB27, reduced the affinity for the receptor 250-fold, and alanine substitution for tryptophan showed a 100-fold reduction in affinity (*29*). When TrpB27 was replaced with phenylalanine, or D-tryptophan, or was oxidized to the oxindole, the affinity was reduced 2−5-fold, indicating that an aromatic interaction is essential for receptor binding. This conclusion is supported by the fact that relaxin will cross-

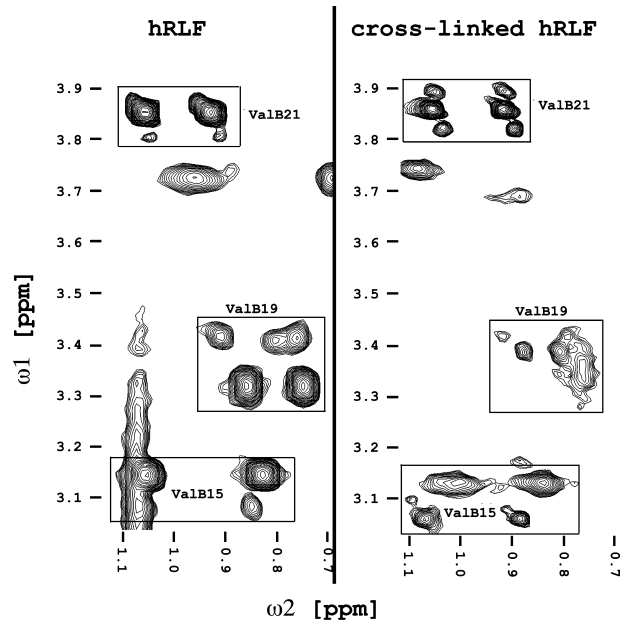

FIGURE 9: Regions of the TOCSY spectra of the hRLF and cross-linked RLF showing the chemical shifts and the multiplicity of the HA−HG cross-peaks for ValB15, ValB19, and ValB21.

react with the RLF receptor only when a tryptophan is present in a position equivalent to TrpB27. Thus, human and porcine relaxins, with Trp in position B27, bind and activate the RLF receptor, whereas rat relaxin with a glycine at position B27 does not (*46*).

However, despite the fact that the indole ring is necessary for high-affinity binding, the solution structures for both the hRLF and the cross-linked RLF show that the binding residues, tryptophan B27 and, in the case of the hRLF, valine B19, are partially buried within a common fold and therefore not readily accessible. Consequently, the dominant solution structures of the hRLF and the cross-linked derivative must represent nonbinding conformers. The binding conformer may be best represented by the minor conformation observed for the cross-linked RLF. Decreased stability of the B chain helix, significant line broadening of the ValB19 side chain, including improved surface exposure of the methyl groups, and two conformations of the indole ring of TrpB27 all imply that a more open structure does exist in addition to the compact fold.

To convert the inactive form (T state) to an active conformation (R state), a partial unfolding must occur prior to receptor binding. Most likely, the T and R states exist in an equilibrium from which the receptor recruits the binding conformer. Therefore, in spite of the different orientation of the tryptophan side chain in the T state of the hRLF and cross-linked RLF (Figure 7), in the R state of the two proteins the indole ring could occupy a very similar position in space. It was suggested that the GGP sequence (B23−B25) functions as a hinge in the orientation of the indole ring (*28, 29*). Indeed, when L-ProB25 was replaced with its D-enantiomer or L-serine, the corresponding RLF derivatives exhibited substantially reduced receptor affinity (*28, 29*).

In this context, it is interesting that within the relaxin/insulin family, insulin also requires a transition from an inactive state prior to insulin−receptor binding. In this transition, the flexibility of the C-terminal region of the insulin B chain is crucial for exposing the binding site. X-ray

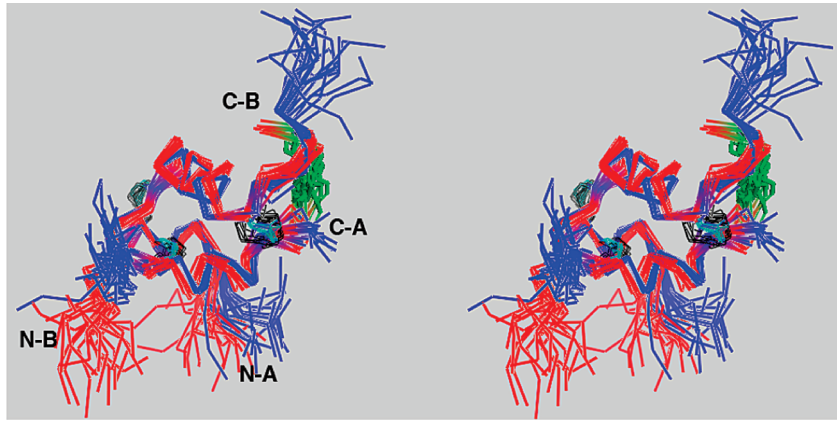

FIGURE 10: Stereoview of the 20 superposed lowest-energy structures of the human RLF (blue) and cross-linked RLF (red). The cross-link is colored green, and the cystine bonds are colored cyan for the hRLF and black for the cross-linked RLF. N-A and N-B represent the N-termini of the A and B chains, respectively. C-A and C-B label the C-termini of the A and B chains, respectively.

(*47*) and NMR data (*48, 49*) of native insulin show that the β-turn (B20−B23) C-terminal of the B chain helix directs residues B24−B28 to the surface of the B chain helix, forming the dimerization site of the insulin hexameric storage form. This fold is maintained in the monomer when dissociating solvents are present (*48, 50*). Molecular dynamic calculations implied that in the virtual insulin monomers the C-terminal portion of the B chain, B25−B30 (equivalent to RLF-residues B28−B33), moves away from the B chain helix to expose the receptor interacting site of the hormone (*51*). Such a movement is supported by structures of nonaggregating insulin mutants with unusually high receptor affinities (*52*−*57*). In insulin, the β-turn (B20−B23, GERG) is stabilized by two characteristic hydrogen bonds, one between the carbonyl oxygen of GlyB20 and the NH proton of GlyB23 and the second between the carbonyl oxygen of CysB19 and the NH proton of ArgB22. In several flexible potent insulin analogues, these H-bonds seem to be absent (*54*) or altered (*56*). Insulins mutated within the B20−B23 β-turn suggest that neither the β-turn geometry nor its local stability correlates with activity, implying that the highly conserved β-turn is not essential for receptor affinity and, in fact, may represent inactive conformers (*58*).

In the RLF, the turn C-terminal to the B chain helix (B23−B26, GGPR) is not a type I β-turn as in insulin because one of the proton donor positions is occupied by proline. Consequently, the C-terminal region of the RLF B chain is oriented differently. Close contacts between the C-terminal region of the B chain and the A chain N-terminal and C-terminal region existing in insulin are absent in the RLF. Even when a cross-linker forces the side chain of residue B26 toward the C-terminus of the A chain, long-range NOEs between the two chains are not observed.

Like the fold of the insulin B chain, the fold of the RLF B chain is stabilized by hydrophobic interactions. In the case of the RLF, this involves the indole ring in position B27 and methyl groups that would otherwise expose a hydrophobic array on the surface of the B chain helix. This RLF-like B chain fold has been reported for human relaxin 3 (insl7), where the relaxin receptor (LGR7) binding site becomes accessible only upon unfolding (*15*). The structural transition required for receptor binding may not be universal for other relaxins as suggested by the X-ray structure of human relaxin 2 (*14*); however, the C-terminal B chain sequence [CGGS(T)RW] in human relaxin 3 (*9, 15*) and tamar, shark, and skate relaxins (*59*) suggests that the C-terminal structural motif is likely to persist in some relaxins. In rat, mouse, guinea pig, hamster, orangutan II, rhesus monkey, and baboon relaxin tryptophan B27 is replaced with an aliphatic residue (*59*), which may not promote this fold. In general, the lack of solution structures and the extraordinary sequence diversity of relaxin (*59*) make it difficult to generalize.

While the hormones insulin, RLF, and relaxin 3 must undergo a similar conformational transition to bind and activate their receptor, information about structural requirements of the corresponding receptor is still limited. Initial observations on ligand binding to LGR7 and LGR8 show some similarities to the better-investigated insulin tyrosine kinase receptor. Svendsen et al. (*26*) reported LGR8 aggregation and negative cooperative binding of the RLF to LGR8 and suggested that for receptor activation the RLF binds to the high-affinity site on one receptor and to the low-affinity site of a second receptor within the aggregate. Such a mechanism is well-established for the activation of the insulin receptor (*60, 61*) where the high-affinity site of the insulin monomer is in contact with fibronectin domain III (FnIII) and the low-affinity site with the second leucine-rich repeat domain (L2) on the opposite monomer in the receptor dimer (*61*−*63*). In terms of difference, the high-affinity site on the RLF and relaxin receptors is located on a contiguous array on the concave surface of the leucine-rich repeat surface (*27, 64*), whereas the low-affinity site might be located on the seven-transmembrane domain (*46*).

In conclusion, NMR data and the solution structure of a fully active cross-linked RLF derivative support the possibility that a transition of a compact nonbinding conformer to a relaxed binding conformer occurs and that such a transition is a frequent mechanism by which hormones of the relaxin/insulin family interact with their corresponding receptors.

ACKNOWLEDGMENT

The 800 MHz spectra were acquired at The Danish Instrument Center for NMR Spectroscopy of Biological Macromolecules. We thank Jens Ø. Duus and Bent O. Petersen for technical assistance.

SUPPORTING INFORMATION AVAILABLE

Experimental chemical shifts, NOEs, and structure coordinates of the hRLF and cross-linked RLF. This material is available free of charge via the Internet at http://pubs.acs.org.

REFERENCES

1. Ryle, A. P., Sanger, F., Smith, L. F., and Kitai, R. (1955) The disulphide bonds of insulin. *Biochem. J. 60*, 541–556.
2. Rinderknecht, E., and Humbel, R. E. (1978) The amino acid sequence of human insulin-like growth factor I and its structural homology with proinsulin. *J. Biol. Chem. 253*, 2769–2776.
3. Schwabe, C., and McDonald, J. K. (1977) Relaxin: A disulfide homolog of insulin. *Science 197*, 914–915.
4. Isaacs, N., James, R., Niall, H., Bryant-Greenwood, G., Dodson, G. G., Evans, A., and North, A. C. T. (1978) Relaxin and its structural relationship to insulin. *Nature 271*, 278–281.
5. Adham, I. M., Burkhardt, E., Benahmed, M., and Engel, W. (1993) Cloning of a cDNA for a novel insulin-like peptide of the testicular Leydig cells. *J. Biol. Chem. 268*, 26668–26672.
6. Chassin, D., Laurent, A., Janneau, J. L., Berger, R., and Bellet, D. (1995) Cloning of a new member of the insulin gene superfamily (INSL4) expressed in human placenta. *Genomics 29*, 465–470.
7. Conklin, D., Lofton-Day, C. E., Haldeman, B. A., Ching, A., Whitmore, T. E., Lok, S., and Jaspers, S. (1999) Identification of INSL5, a new member of the insulin superfamily. *Genomics 60*, 50–56.
8. Kasik, J., Muglia, L., Stephan, D. A., and Menon, R. K. (2000) Identification, chromosomal mapping, and partial characterization of mouse insl6: A new member of the insulin family. *Endocrinology 141*, 458–461.
9. Bathgate, R. A. D., Samuel, C. S., Burazin, T. C. D., Layfield, S., Laasz, A. A., Reytomas, I. G. T., Dawson, N. F., Zhao, C., Bond, C., Summers, R. J., Parry, L. J., Wade, J. D., and Tregear, G. W. (2002) Human relaxin gene 3 (H3) and the equivalent mouse relaxin (M3) gene: Novel members of the relaxin peptide family. *J. Biol. Chem. 277*, 1148–1157.
10. Liu, C., Eriste, E., Sutton, S., Chen, J., Roland, B., Kuei, C., Farmer, N., Joernvall, H., Sillard, R., and Lovenberg, T. W. (2003) Identification of relaxin-3/INSL7 as an endogenous ligand for the orphan G-protein-coupled receptor GPCR135. *J. Biol. Chem. 278*, 50754–50764.
11. Blundell, T., Cutfield, J. F., Cutfield, S. M., Dodson, E. G., Dodson, G. G., Hodgkin, D., Mercola, D. A., and Vijayan, M. (1971) Atomic positions in rhombohedral 2-zinc insulin crystals. *Nature 231*, 506–511.
12. Sato, A., Nishimura, S., Ohkubo, T., Kyogoku, Y., Koyama, S., Kobayashi, M., Yasuda, T., and Kobayashi, Y. (1993) Three-dimensional structure of human insulin-like growth factor-I (IGF-I) determined by ^{1}H-NMR and distance geometry. *Int. J. Pept. Protein Res. 41*, 433–440.
13. Torres, A. M., Forbes, B. E., Aplin, S. E., Wallace, J. C., Francis, G. L., and Norton, R. S. (1995) Solution structure of human insulin-like growth factor II. Relationship to receptor and binding protein interactions. *J. Mol. Biol. 248*, 385–401.
14. Eigenbrot, C., Randal, M., Quan, C., Burnier, J., O'Connell, L., Rinderknecht, E., and Kossiakoff, A. A. (1991) X-ray structure of human relaxin at 1.5 Å: Comparison to insulin and implications for receptor binding determinants. *J. Mol. Biol. 221*, 15–21.
15. Rosengren, K. J., Lin, F., Bathgate, R. A. D., Tregear, G. W., Daly, N. L., Wade, J. D., and Craik, D. J. (2006) Solution structure and novel insight into determinants of receptor specificity of human relaxin-3. *J. Biol. Chem. 281*, 5845–5851.
16. Rosengren, K. J., Zhang, S., Lin, F., Daly, N. L., Scott, D. J., Hughes, R. A., Bathgate, R. A., Craik, D. J., and Wade, J. D. (2006) Solution structure and characterization of the receptor binding surface of insulin-like peptide 3. *J. Biol. Chem. 281*, 28287–28295.
17. Ullrich, A., Bell, J. R., Chen, E. Y., Herrera, R., Petruzzelli, L. M., Dull, T. J., Gray, A., Coussens, L., Liao, Y. C., Tsubokawa, M., Mason, A., Seeburg, P., Grunfeld, C., Rosen, O. M., and Ramachandran, J. (1985) Human insulin receptor and its relationship to the tyrosine kinase family of oncogenes. *Nature 313*, 756–761.
18. Ebina, Y., Ellis, L., Jarnagin, K., Edery, M., Graf, L., Clauser, E., Ou, J. H., Masiarz, F., Kan, Y. W., Goldfine, I. D., Roth, R. A., and Rutter, W. J. (1985) The human insulin receptor cDNA: The structural basis for hormone-activated transmembrane signalling. *Cell 40*, 747–758.
19. Ullrich, A., Gray, A., Tam, A. W., Yang-Feng, T., Tsubokawa, M., Collins, C., Henzel, W., Le Bon, T., Kathuria, S., Chen, E., Jacobs, S., Francke, U., Ramachandran, J., and Fujita-Yamaguchi, Y. (1986) Insulin-like growth factor I receptor primary structure: Comparison with insulin receptor suggests structural determinants that define functional specificity. *EMBO J. 5*, 2503–2512.
20. Overbeek, P. A., Gorlov, I. P., Sutherland, R. W., Houston, J. B., Harrison, W. R., Boetther-Tong, H. L., Bishop, C. E., and Agoulnik, A. I. (2001) A transgenic insertion causing cryptorchidism in mice. *Genesis 30*, 26–35.
21. Hsu, S. Y., Nakabayashi, K., Nishi, S., Kumagai, J., Kudo, M., Sherwood, O. D., and Hsueh, A. J. W. (2002) Activation of orphan receptors by the hormone relaxin. *Science 295*, 671–674.
22. Liu, C., Chen, J., Sutton, S., Roland, B., Kuei, C., Farmer, N., Sillard, R., and Lovenberg, T. W. (2003) Identification of relaxin-3/INSL7 as a ligand for GPCR142. *J. Biol. Chem. 278*, 50765–50770.
23. Adham, I. M., and Agoulnik, A. I. (2004) Insulin-like 3 signalling in testicular descent. *Int. J. Androl. 27*, 257–265.
24. Büllesbach, E. E., and Schwabe, C. (2002) The primary structure and the disulfide links of the bovine relaxin-like factor (RLF). *Biochemistry 41*, 274–281.
25. Büllesbach, E. E., and Schwabe, C. (2004) Synthetic cross-links arrest the C-terminal region of the relaxin-like factor (RLF) in an active conformation. *Biochemistry 43*, 8021–8028.
26. Svendsen, A. M., Vrecl, M., Ellis, T. M., Heding, A., Kristensen, J. B., Wade, J. D., Bathgate, R. A., De Meyts, P., and Nohr, J. (2008) Cooperative binding of insulin-like peptide 3 to a dimeric relaxin family peptide receptor 2. *Endocrinology 149*, 1113–1120.
27. Scott, D. J., Wilkinson, T., Zhang, S., Ferraro, T., Wade, J., Tregear, G. W., and Bathgate, R. A. (2007) Defining the LGR8 residues involved in binding insl3. *Mol. Endocrinol. 21*, 1699–1713.
28. Büllesbach, E. E., and Schwabe, C. (2006) The mode of interaction of the relaxin-like factor (RLF) with the leucine-rich repeat G protein-activated receptor 8. *J. Biol. Chem. 281*, 26136–26143.
29. Büllesbach, E. E., and Schwabe, C. (1999) Tryptophan B27 in the relaxin-like factor (RLF) is crucial for RLF receptor binding. *Biochemistry 38*, 3073–3078.
30. Piotto, M., Saudek, V., and Sklenar, V. (1992) Gradient-tailored excitation for single-quantum NMR spectroscopy of aqueous solutions. *J. Biomol. NMR 2*, 661–665.
31. Rance, M., Sørensen, O. W., Bodenhausen, G., Wagner, G., Ernst, R. R., and Wuthrich, K. (1983) Improved spectral resolution in COSY ^{1}H NMR spectra of proteins via double quantum filtering. *Biochem. Biophys. Res. Commun. 117*, 479–485.
32. Jeener, J., Meier, B. H., Bachmann, P., and Ernst, R. R. (1979) Investigation of exchange processes by two-dimensional NMR spectroscopy. *J. Chem. Phys. 71*, 4546.
33. Macura, S., Huang, Y., Suter, D., and Ernst, R. R. (1981) Two-dimensional chemical exchange and cross-relaxation spectroscopy of coupled nuclear spins. *J. Magn. Reson. 43*, 259–281.
34. Braunschweiler, L., and Ernst, R. R. (1983) Coherence transfer by isotopic mixing application to proton correlation spectroscopy. *J. Magn. Reson. 53*, 521–528.
35. Bax, A., and Davis, D. G. (1985) MLEV-17-based two-dimensional homonuclear magnetization transfer spectroscopy. *J. Magn. Reson. 65*, 355–360.
36. Delaglio, F., Grzesiek, S., Vuister, G. W., Zhu, G., Pfeifer, J., and Bax, A. (1995) NMRPipe: A multidimensional spectral processing system based on UNIX pipes. *J. Biomol. NMR 6*, 277–293.
37. Wüthrich, K. (1986) *NMR of proteins and nucleic acids*, Wiley and Sons, New York.
38. Wishart, D. S., Sykes, B. D., and Richards, F. M. (1992) The chemical shift index: A fast and simple method for the assignment of protein secondary structure through NMR spectroscopy. *Biochemistry 31*, 1647–1651.
39. Baxter, N. J., and Williamson, M. P. (1997) Temperature dependence of ^{1}H chemical shifts in proteins. *J. Biomol. NMR 9*, 359–369.
40. Kristensen, S. M., Sørensen, M. D., Gesmar, H., and Led, J. J. (1996) Estimation of signal intensities in 2D NMR spectra with severe basline distortion by combined linear-prediction and least-square analyses. *J. Magn. Reson., Ser. B 112*, 193.
41. Berjanskii, M. V., Neal, S., and Wishart, D. S. (2006) PREDITOR: A web server for predicting protein torsion angle restraints. *Nucleic Acids Res. 34*, W63–W69.
42. Barsukov, I. L., and Lian, L. Y. (1993) Structure determination from NMR data. I Analysis of NMR data. In *NMR of macromol-*

ecules: A practical approach (Roberts, G. C. K., Ed.) pp 315−358, IRL Press, Oxford, U.K.

43. Rieping, W., Habeck, M., Bardiaux, B., Bernard, A., Malliavin, T. E., and Nilges, M. (2007) ARIA2: Automated NOE assignment and data integration in NMR structure calculation. *Bioinformatics 23*, 381–382.
44. Schwieters, C. D., Kuszewski, J. J., Tjandra, N., and Clore, G. M. (2003) The Xplor-NIH NMR molecular structure determination package. *J. Magn. Reson. 160*, 65–73.
45. Nilges, M., and O'Donoghue, S. I. (1998) Ambiguous NOE and automated NOE assignment. *Prog. Nucl. Magn. Reson. Spectrosc. 32*, 107–139.
46. Halls, M. L., Bond, C. P., Sudo, S., Kumagai, J., Ferraro, T., Layfield, S., Bathgate, R. A., and Summers, R. J. (2005) Multiple binding sites revealed by interaction of relaxin family peptides with native and chimeric relaxin family peptide receptors 1 and 2 (LGR7 and LGR8). *J. Pharmacol. Exp. Ther. 313*, 677–687.
47. Baker, E. N., Blundell, T. L., Cutfield, J. F., Cutfield, S. M., Dodson, E. J., Dodson, G. G., Crowfoot Hodgkin, D. M., Hubbard, R. E., Isaacs, N. W., Reynolds, C. D., Sakabe, K., Sakabe, N., and Vijayan, N. M. (1988) The structure of 2Zn pig insulin crystals at 1.5 Å resolution. *Philos. Trans. R. Soc. London, Ser. B 319*, 369–456.
48. Hua, Q. X., and Weiss, M. A. (1991) Comparative 2D NMR studies of human insulin and des-pentapeptide insulin: Sequential resonance assignment and implications for protein dynamics and receptor recognition. *Biochemistry 30*, 5505–5515.
49. Chang, X., Jorgensen, A. M., Bardrum, P., and Led, J. J. (1997) Solution structures of the R6 human insulin hexamer. *Biochemistry 36*, 9409–9422.
50. Bocian, W., Sitkowski, J., Bednarek, E., Tarnowska, A., Kawecki, R., and Kozerski, L. (2008) Structure of human insulin monomer in water/acetonitrile solution. *J. Biomol. NMR 40*, 55–64.
51. Zoete, V., Meuwly, M., and Karplus, M. (2004) A comparison of the dynamic behavior of monomeric and dimeric insulin shows structural rearrangements in the active monomer. *J. Mol. Biol. 342*, 913–929.
52. Mirmira, R. G., and Tager, H. S. (1989) Role of the phenylalanine B24 side chain in directing insulin interaction with its receptor: Importance of main chain conformation. *J. Biol. Chem. 264*, 6349–6354.
53. Weiss, M. A., Hua, Q. X., Lynch, C. S., Frank, B. H., and Shoelson, S. E. (1991) Heteronuclear 2D NMR studies of an engineered insulin monomer: Assignment and characterization of receptor-binding surface by selective ^{2}H and ^{13}C labeling with application to protein design. *Biochemistry 30*, 7373–7389.
54. Hua, Q. X., Shoelson, S. E., Kochoyan, M., and Weiss, M. A. (1991) Receptor binding redefined by a structural switch in a mutant human insulin. *Nature 354*, 238–241.
55. Hua, Q. X., Kochoyan, M., and Weiss, M. A. (1992) Structure and dynamics of des-pentapeptide-insulin in solution: The molten-globule hypothesis. *Proc. Natl. Acad. Sci. U.S.A. 89*, 2379–2383.
56. Jørgensen, A. M. M., Olsen, H. B., Balschmidt, P., and Led, J. J. (1996) Solution structure of the superactive monomeric des-[Phe(B25)] human insulin mutant: Elucidation of the structural basis for the monomerization of des-[Phe(B25)] insulin and the dimerization of native insulin. *J. Mol. Biol. 257*, 684–699.
57. Keller, D., Clausen, R., Josefsen, K., and Led, J. J. (2001) Flexibility and bioactivity of insulin: An NMR investigation of the solution structure and folding of an unusually flexible human insulin mutant with increased biological activity. *Biochemistry 40*, 10732–10740.
58. Nakagawa, S. H., Hua, Q. X., Hu, S. Q., Jia, W., Wang, S., Katsoyannis, P. G., and Weiss, M. A. (2006) Chiral mutagenesis of insulin. Contribution of the B20-B23 β-turn to activity and stability. *J. Biol. Chem. 281*, 22386–22396.
59. Schwabe, C., and Büllesbach, E. E. (1998) *Relaxin and the fine structure of proteins*, pp 13−23, Springer, New York.
60. De Meyts, P., Bianco, A. R., and Roth, J. (1976) Site-site interactions among insulin receptors: Characterization of the negative cooperativity. *J. Biol. Chem. 251*, 1877–1888.
61. De Meyts, P. (2008) The insulin receptor: A prototype for dimeric, allosteric membrane receptors? *Trends Biochem. Sci. 33*, 376–384.
62. McKern, N. M., Lawrence, M. C., Streltsov, V. A., Lou, M. Z., Adams, T. E., Lovrecz, G. O., Elleman, T. C., Richards, K. M., Bentley, J. D., Pilling, P. A., Hoyne, P. A., Cartledge, K. A., Pham, T. M., Lewis, J. L., Sankovich, S. E., Stoichevska, V., Da Silva, E., Robinson, C. P., Frenkel, M. J., Sparrow, L. G., Fernley, R. T., Epa, V. C., and Ward, C. W. (2006) Structure of the insulin receptor ectodomain reveals a folded-over conformation. *Nature 443*, 218–221.
63. Ward, C., Lawrence, M., Streltsov, V., Garrett, T., McKern, N., Lou, M. Z., Lovrecz, G., and Adams, T. (2008) Structural insights into ligand-induced activation of the insulin receptor. *Acta Physiol. 192*, 3–9.
64. Büllesbach, E. E., and Schwabe, C. (2005) The trap-like relaxin-binding site of the leucine-rich G-protein-coupled receptor 7. *J. Biol. Chem. 280*, 14051–14056.

BI801412W